Compliant Mechanisms That Use Static Balancing to Achieve Dramatically Different States of Stiffness

Kuppens, P. R.; Bessa, M. A.; Herder, J. L.; Hopkins, J. B.

DOI
10.1115/1.4049438

Publication date
2021

Document Version
Final published version

Published in
Journal of Mechanisms and Robotics

Compliant Mechanisms That Use Static Balancing to Achieve Dramatically Different States of Stiffness

P. R. Kuppens[1]
Mechatronic System Design Precision and Microsystems Engineering,
Delft University of Technology,
Zuid Holland, Delft 2628 CD, The Netherlands
e-mail: p.r.kuppens@tudelft.nl

M. A. Bessa
Materials Science and Engineering,
Delft University of Technology,
Zuid Holland, Delft 2628 CD, The Netherlands
e-mail: M.A.bessa@tudelft.nl

J. L. Herder
Mechatronic System Design Precision and Microsystems Engineering,
Delft University of Technology,
Zuid Holland, Delft 2628 CD, The Netherlands
e-mail: J.L.herder@tudelft.nl

J. B. Hopkins
Mechanical and Aerospace Engineering,
University of California, Los Angeles,
Los Angeles, CA 90095
e-mail: hopkins@seas.ucla.edu

Stiffness in compliant mechanisms can be dramatically altered and even eliminated entirely by using static balancing. This requires elastic energy to be inserted before operation, which is most often done with an additional device or preloading assembly. Adding such devices contrasts starkly with primary motivations for using compliant mechanisms, such as part count reduction, increased precision, and miniaturization. However, statically balanced compliant mechanisms with a fully monolithic architecture are scarce. In this article, we introduce two novel statically balanced compliant mechanisms with linear and rotary kinematics that do not require preloading assembly, enabling miniaturization. Static balance is achieved by the principle of opposing constant force and extended to a rotational device by using opposing constant torque mechanisms for the first time. A constant force mechanism based on existing work is used and inspired a novel constant torque mechanism. A single-piece device is obtained by monolithically integrating a bistable switch for preloading, which allows static balance to be turned on and off. The linear device reduces stiffness by 98.5% over 10 mm, has significantly reduced device complexity and has doubled relative range of motion from 3.3% to 6.6% compared to the state of the art. The rotary device reduces stiffness by 90.5% over 0.35 rad.
[DOI: 10.1115/1.4049438]

Keywords: compliant mechanisms, static balancing, stiffness reduction, mechanism design

1 Introduction

Fully compliant mechanisms (CMs) improve upon their multi-component rigid-body counterparts in many respects. Their monolithic nature increases precision and reliability, reduces friction and wear, and eliminates assembly that makes them perfect for micro-scale applications in, for example, MEMS [1–7] and laparoscopic surgical tools [8–11].

However, they store a significant part of the input energy as strain energy because their functionality arises from deformation of slender segments. This may reduce range of motion, hamper energy efficiency, or cause high natural frequencies [12]. This inherent and often undesired stiffness may be compensated for by adding an equal but opposite negative stiffness in parallel.

An isolated mechanism with negative stiffness is unstable and requires some form of preloading. During preloading, potential elastic energy is inserted into the device. Upon motion, energy flows out of the unstable negative stiffness part and enters the stable part with positive stiffness, keeping the total elastic potential energy constant. It follows that all internal forces are in sustained static equilibrium. Hence, these systems are called statically balanced.

Preloading is often done manually [13,14] but can also be done as part of the manufacturing process in small-scale devices such as MEMS [15]. Manual preloading often relies on a preloading assembly, an external device using for example screw lead. This contrasts starkly with the motivation for using CM in the first place and eliminates any possibility for miniaturization.

Few examples of CM without preloading assembly exist. Among them are a fully compliant gripper [16] and linear stage [17,18] with on and off switch, a linear stage based on multistable mechanisms [19], and a statically balanced linear stage preloaded once with hooks [20]. Some of the aforementioned examples have relatively complicated geometry, limiting the ratio between device footprint and range of motion. Some use contact between components to ensure preloading and some are not properly constrained. All aforementioned examples only consider rectilinear motion, and it is not immediately obvious how a rotational system could be devised.

In this article, we introduce two novel statically balanced fully compliant mechanisms with rectilinear and rotational kinematics that do not require a preloading assembly. In the linear case, static balance is reversibly achieved by the principle of opposing constant force (OCF), first introduced by Refs. [17,18]. We use a constant force mechanism (CFM) based on the work from Ref. [15], resulting in statically balanced compliant mechanism with reduced complexity and improved range of motion compared to Ref. [17,18]. We have expanded the principle of OCF to rotary devices by using opposing constant torque (OCT) mechanisms for the first time. A novel constant torque mechanism (CTM) is used that is based on the same principles as the constant force mechanism from Ref. [15]. A monolithic architecture is achieved by integrating a fully compliant bistable switch for preloading. Toggling the bistable switch allows static balance to be turned on and off, effectively switching between high and low stiffness configurations.

The mechanisms presented may find applications in low-frequency sensor technology [4] and low-frequency mechanical energy harvesters [21] and make compliant micro transmission mechanisms more efficient [7,22]. In addition, they may be perfect for protecting sensitive instruments for space applications. Upon launch, the high stiffness provides robustness and protection. Once in orbit, the highly sensitive and compliant state may be activated.

[1]Corresponding author.

Contributed by the Mechanisms and Robotics Committee of ASME for publication in the Journal of Mechanisms and Robotics. Manuscript received March 4, 2020; final manuscript received November 14, 2020; published online January 22, 2021. Assoc. Editor: Zhong You.

2 Balancing Method

Static balancing can be done in two distinctive ways. By far the most common and well-known approach is to add a spring with negative stiffness in parallel to the functional positive stiffness part [8,10,15,23].

A second and less frequently used method opposes two constant forces. In a CFM force is constant over some part of its motion domain. By preloading two such mechanisms against each other, the constant forces cancel out resulting in zero force. The only mechanism to exploit this principle of OCF for stiffness reduction is reported in Refs. [16,18].

2.1 Opposing Constant Force. A balanced system can be created by preloading two CFMs against each other. A graphical explanation is shown in Fig. 1. The dashed and dotted curves are force (F) deflection (u) characteristics of two CFMs with their degree-of-freedom in the opposite direction.

If left unconnected, one CFM (dotted) will have positive constant force if moved to the right. The other CFM (dashed) will have negative constant force if moved to the left. By connecting the CFMs in parallel, the force deflection can be simply added to uncover the combined behavior. If done in their undeformed state, the high stiffness away from the constant force domain is dominant. The combined stiffness is therefore very high, as shown by the solid line in Fig. 1(*a*).

When both CFMs are displaced over half their motion domain when unconnected, their stiffness curves essentially slide over each other. By connecting them in this preloaded state, the positive and negative constant forces cancel out resulting in the solid curve in Fig. 1(*b*).

The concept of OCF can be easily extended to rotational devices by considering an OCT mechanism. Connecting two preloaded CTMs in parallel cancels the constant torques in exactly the same way.

Fabricated mechanisms with OCF and OCT in their stiff and compliant configuration are shown in Fig. 2. In each case, the mechanisms are connected with an insert with dovetails. As a monolithic alternative bistable mechanisms will replace these inserts.

2.2 Constant Force and Torque Mechanisms. A CFM is created when a positive stiffness is combined in parallel with a bistable mechanism [24,25]. In Refs. [24,25], these components can be individually identified. However, in Ref. [15], a constant force mechanism is reported where no such distinction can be made.

It is composed of two parallel plate springs, to form a simple linear stage, and an additional plate spring at the bottom, initially overconstraining the system. A thermally induced expansion of all plate springs is used to compute the first buckling mode shape

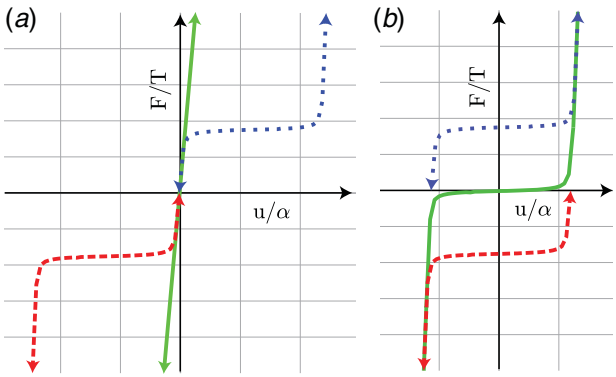

Fig. 1 Principle of static balance by opposing constant force and torque: (*a*) force (F) and torque (T) versus deflection (u) and angular displacement (α) in the stiff configuration and (*b*) the compliant configuration

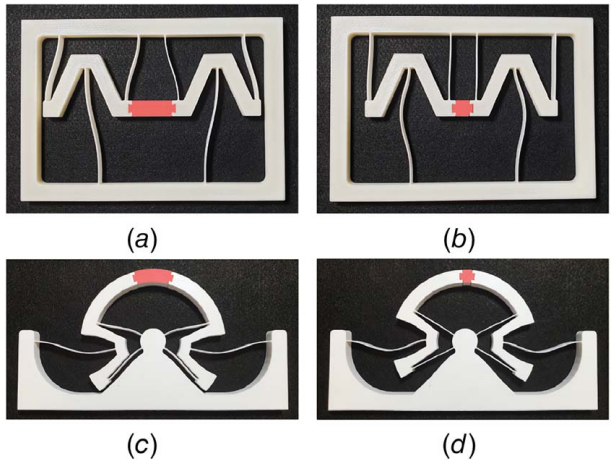

Fig. 2 Photos of 3D printed OCF and OCT mechanisms with dovetail inserts in stiff and compliant configuration: (*a*) OCF stiff, (*b*) OCF compliant, (*c*) OCT stiff, and (*d*) OCT compliant

with a linear buckling analysis. The constant force mechanisms is obtained by assuming a scaled version of this shape as new geometry.

Scaling the solution of the buckling analysis allows control over the size of the low stiffness domain and magnitude of the constant force. The length of the plate spring at the bottom (parameters L_{ns} and r_{ns} in Fig. 5) allows control over the slope of the low stiffness domain. For short plate springs, the slope over the low stiffness range becomes negative and for long plate springs positive [15]. Its length is chosen right where behavior transitions from a negative to positive slope, resulting in minimal stiffness. A simulation and a measurement of the CFM are shown in Fig. 3(*a*).

Various CTMs can be found in literature [26,27]. Both these mechanisms rely on shape optimized radial plate springs with

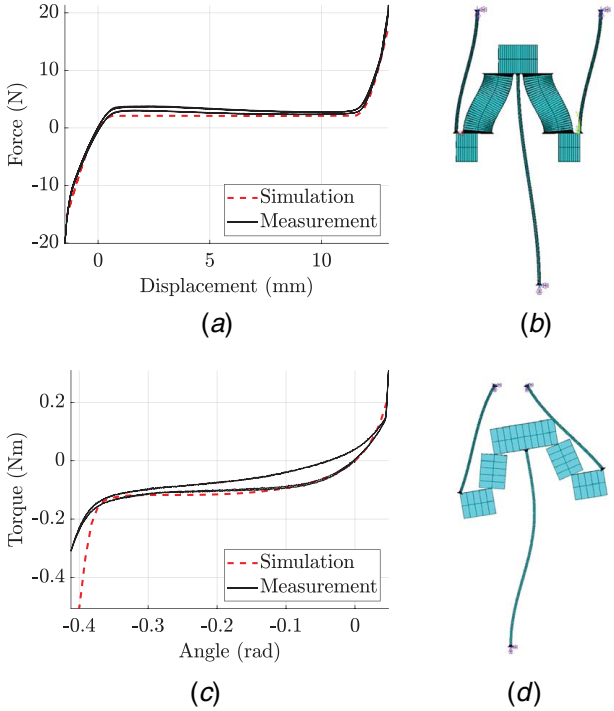

Fig. 3 Constant force and torque mechanisms: (*a*) simulation and measurement of the CFM, (*b*) finite element model of CFM, (*c*) simulation and measurement of CTM, and (*d*) finite element model of CTM

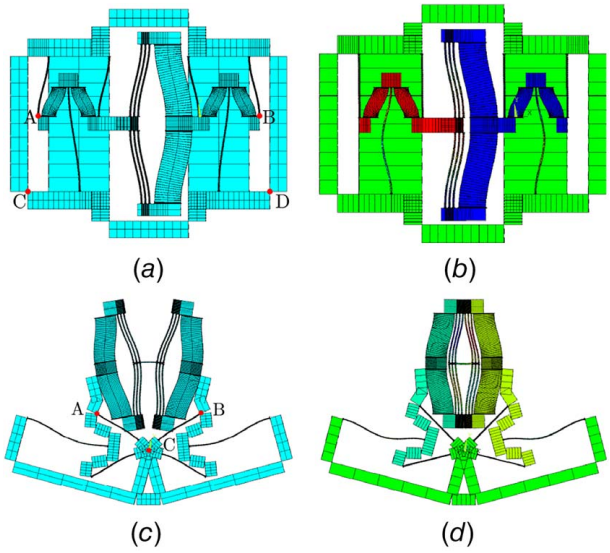

Fig. 4 Finite element models: (*a*) undeformed element plot of OCF mechanism, (*b*) displacement solution of OCF mechanism, (*c*) undeformed element plot of OCT mechanism, and (*d*) displacement solution of OCT mechanism

complex geometry. What we propose instead is a slight modification of the CFM from [15]. FACT [28,29] tells us that an instantaneous center of rotation is created at the point of virtual intersection of two plate springs. Parallel plate springs, which intersect at infinity, will therefore cause rectilinear motion. Rotation is simply obtained by tilting the plate springs inwards, see Fig. 3(*d*). Constant torque behavior is obtained by computing the first buckling mode shape and assuming a scaled version of this shape to be the new geometry. A simulation and a measurement of the CTM is shown in Fig. 3(*c*).

2.3 Preloading Mechanisms. A monolithic alternative to the inserts with dovetails from Fig. 2 is to use a bistable mechanism. A bistable mechanism has two stable configurations, can stay in either equilibrium indefinitely, and can be switched reversibly. One equilibrium (the as fabricated configuration) will replace the long insert, and the other will replace the short insert.

Many fully compliant bistable mechanisms are reported in the literature, both macro- and micro-scale and both translational [30,31] and rotational [32,33]. In this article, we will use bistable mechanisms similar to Ref. [31] since they are proven to work on micro-scale. The shape of these curved-beam bistable elements is given by

$$w(x) = \frac{h}{2}\left[1 - \cos\left(2\pi\frac{x}{L}\right)\right] \tag{1}$$

where h is the amplitude or initial apex of the beam and L is the total length and $x \in [0, L]$.

If boundary conditions are infinitely stiff each additional bistable element in parallel adds to an increased magnitude of the bistability. However, since more bistable elements in parallel also increase the force on the boundaries, there is a limit to the number of bistable elements in practice. We found that a total number of three parallel bistable elements worked well in this design.

2.4 Finite Element Models. Both the individual CFM and CTM and fully compliant OCF and OCT mechanisms are modeled in ANSYS APDL. A parametric model is built with beam188 elements, and all simulations are displacement controlled. A Young's modulus of 3.12 GPa is used with a Poisson's ratio of 0.3 [34].

To determine the shape of the CFM and CTM, all elements are given an arbitrary coefficient of thermal expansion of

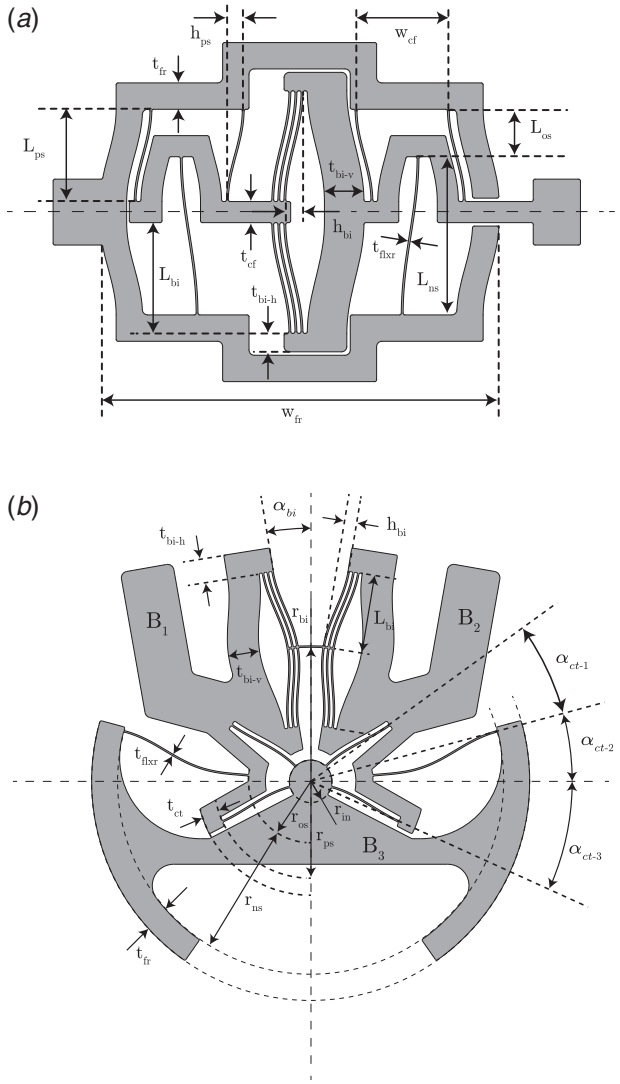

Fig. 5 Annotated CAD drawings with dimensions of (*a*) the OCF mechanism and (*b*) the OCT mechanism

$5 \times 10^{-6}\ ^{\circ}\mathrm{C}^{-1}$. A linear buckling analysis is then performed under a uniform temperature of $1\ ^{\circ}\mathrm{C}$ to get the first buckling mode shape. The resulting normalized mode shapes are then scaled and used as undeformed geometry. The CFM are scaled to an amplitude of 6 mm and the CTM to 9.5 deg. Next bistable mechanisms are constructed, resulting in the geometry given by Figs. 4(*a*) and 4(*c*).

To simulate postbuckling behavior, imperfections are required. In each case, the first four normalized buckling mode shapes are computed and added to the nodal coordinates with a scaling of 0.01. To compute this, point C of the OCF mechanism (see Fig. 4(*a*)) is constrained in all directions and point D is constrained in the y-direction. A unit force is applied at points A and B pointing toward each other. For the OCT mechanism, A and C are fully constrained, while a unit torque is applied at B.

Figures 4(*b*) and 4(*d*) show a displacement solution after the bistable switches have been activated, and the mechanism is moved to the middle of the motion domain. In both cases, this is done by first fully constraining points A and then moving B toward A. Once through the bistability, A is released and B is moved back to its starting position.

2.5 Final Mechanism Design and Manufacturing. Dimensions from the parametric model are transferred to a 3D CAD drawing. All mechanisms have a thickness of 7 mm and all plate

Table 1 Parameter values as shown in Fig. 5

CFM		CTM	
Parameter	Value	Parameter	Value
L_{ps}	35 mm	r_{ps}	45 mm
L_{ns}	60 mm	r_{ns}	62 mm
L_{bi}	42 mm	r_{bi}	63.3 mm
L_{os}	10 mm	r_{in}	10 mm
h_{ps}	6 mm	r_{os}	29.3 mm
h_{bi}	6.5 mm	L_{bi}	37 mm
t_{cf}	8 mm	h_{bi}	5.7 mm
t_{bi-v}	15 mm	t_{ct}	8 mm
t_{bi-h}	7 mm	t_{bi-v}	15 mm
t_{fr}	10 mm	t_{bi-h}	11 mm
t_{flxr}	0.7 mm	t_{fr}	12 mm
w_{cf}	35 mm	t_{flxr}	0.7 mm
w_{fr}	151.2 mm	α_{bi}	9.5 deg
		α_{ct-1}	20.5 deg
		α_{ct-2}	15 deg
		α_{ct-3}	24.5 deg

springs a thickness T_{flxr} of 0.7 mm providing a sufficient aspect ratio for out-of-plane stiffness. A fillet is added to each corner with radius 0.7 mm to reduce stress concentrations. In some places, bigger fillets are created for aesthetic purposes.

In each case, the length (L_{ps} and $r_{ps} - r_{in}$) of the plate springs of the stage, responsible for the kinematics, are 35 mm long before buckling mode shapes are computed. Since the analysis is linear, the scaled mode shapes will have plate springs that are slightly longer. Annotated CAD drawings of the OCF and OCT mechanisms are shown in Fig. 5. The dimensions are given in Table 1.

The mechanisms are 3D printed by fused deposition modeling (FDM) on an Original Prusa i3 MK3S out of polylactic acid (PLA) with default printer and slicing settings (Fig. 6). Isotropic material properties are assumed based on FDM-printed PLA with a layer raster angle of 0 deg [34]. A Young's modulus of 3.12 GPa and an ultimate tensile stress of 50.23 MPa are used with a Poison's ratio of 0.3.

2.6 Measurements. Force deflection measurements are done with an Instron 5966 tensile test bench. All mechanisms are

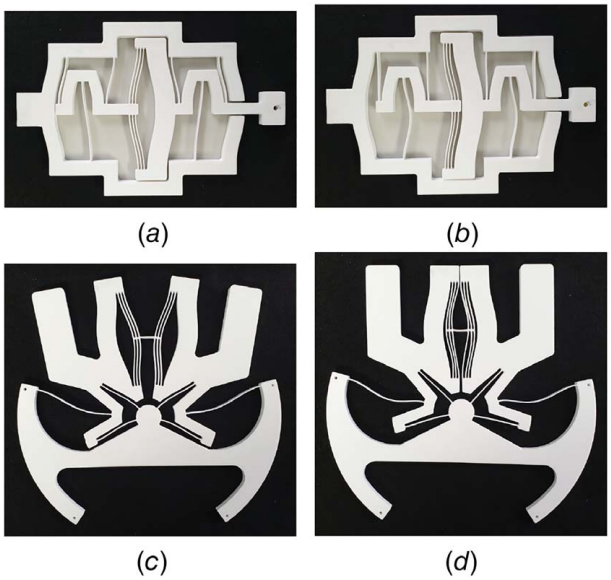

Fig. 6 Photographs of the 3D printed OCF and OCT mechanisms. The OCF mechanism is shown in a (*a*) stiff and (*b*) compliant configuration. The OCT mechanism in shown in a (c) stiff and (*d*) compliant configuration.

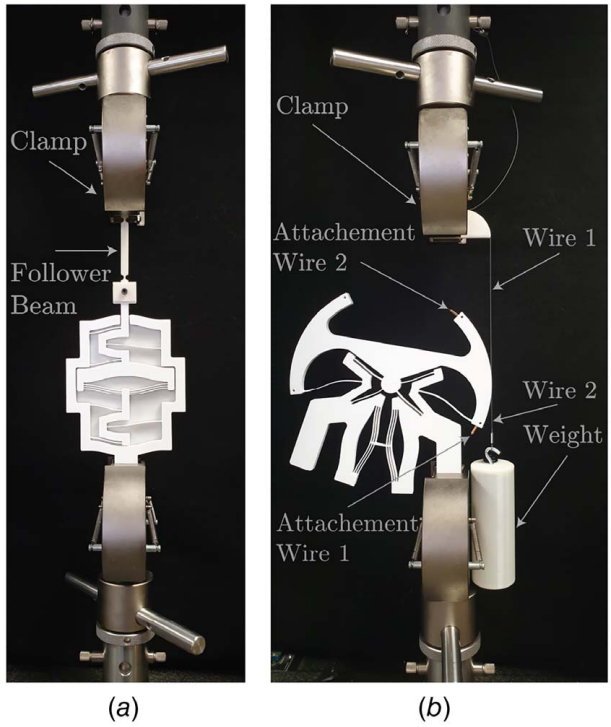

Fig. 7 An (*a*) OCF and (*b*) OCT mechanism clamped in the tensile test bench

cyclically measured in the motion direction for five cycles. Strain rate is 15 mm/min and force is bounded.

An additional follower beam is added between the Instron and the translational device to account for parasitic motion, see Fig. 7(*a*). Torque and angular displacement are measured in the same tensile test bench. A circular arm is attached to the rotational stage centered around the initial center of rotation. Two steel wires run through grooves at the outside of the arm. The wire that runs up is attached to the Instron. The wire that runs down is attached to a 10.2 N weight for preloading because wires can only pull. Since the radius is known (assumed to be constant), the measured displacement and force can be converted into angular displacement and torque. Both measurements are shown in Fig. 8.

Each measurement starts with the mechanism in the stiff configuration. The Instron is used to simultaneously actuate and measure the devices. We first measure the stiff configuration and transition to the compliant state by pushing or pulling through the bistable switches.

3 Results

Figure 8(*g*) shows the experimental (EXP) results and the results from finite element analysis (FEA) of the OCF mechanism transitioning from high to low stiffness. High and low stiffness are indicated with dotted lines, which are obtained by locally fitting the data with least squares. The actuation stiffness is reduced by 98.75% from 14.47 N/mm to −0.18 N/mm with an absolute range of motion of approximately 10 mm and a relative range of motion of 6.6% with respect to the frame width $w_{fr} = 151.2$ mm. Transition by toggling the bistable switch requires 17.71 N as shown by the peak at 2.5 mm.

Figure 8(*h*) shows the angle moment measurement (EXP) and the simulation (FEA) of the OCT mechanism transitioning from stiff to compliant. The angular actuation stiffness is reduced by 90.5% from 3.99 N m/rad to 0.38 N m/rad with a range of motion of approximately 0.35 rad. Transition requires two bistable switches to toggle, shown as the two peaks with values of 1.15 N m and 1.26 N m at, respectively, 0.1 rad and 0.27 rad.

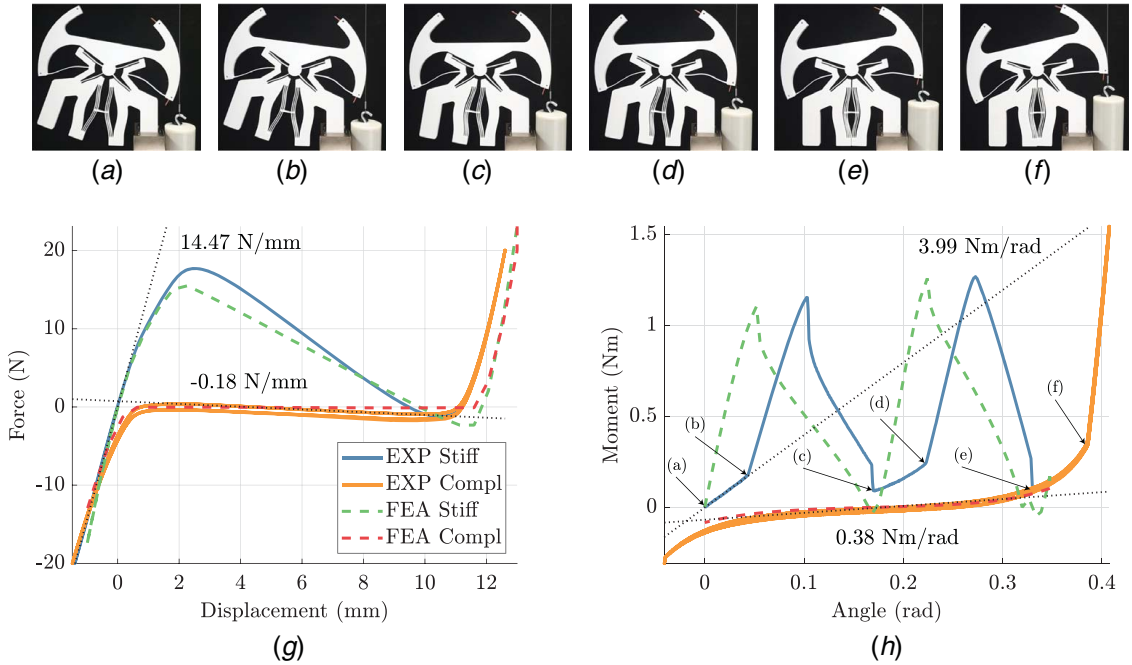

Fig. 8 Experimental (EXP) and finite element analysis (FEA) results of (*g*) CFM and (*h*) CTM mechanisms. In both cases, the transition from stiff to compliant is shown. (*a*)–(*f*) Specific moment of contact and release and correspond to the labels shown in (*h*). High and low stiffness is indicated with the dotted lines, and they are locally fitted to the data with least squares. (*g*) Force displacement of OCF. (*h*) Torque angular displacement of OCT.

Both simulations are in good agreement with measurements. However, in the rotary mechanism, a clear shift and some discontinuities can be observed in the two peaks. Both discrepancies can be explained by repeated contact and release between bodies B_2 and B_3 (see Fig. 5(*b*)) that is not simulated. In simulation, body B_2 is rotated toward body B_1, while B_1 and B_3 are fully constrained. In measurement, however, B_3 is rotated toward B_1, while B_2 is free floating. Because of this, B_2 will have repeated contact and release with body B_3. The events of contact and release are illustrated in Figs. 8(*a*)–8(*f*) and annotated in Fig. 8(*h*).

4 Discussion

We have demonstrated two fully compliant monolithic architectures that have dramatically different states of stiffness. Reversible static balancing is achieved by opposing two constant force and torque mechanisms with bistable mechanisms. We used constant force mechanisms based on Ref. [15], but instead of inducing buckling in combination with annealing, we directly manufactured the buckling mode shape stress free. The same was done to create a novel constant torque mechanism.

A negative low stiffness for the device with rectilinear motion is reported in Fig. 8(*g*) and Sec. 3. The stiffness is negative because the individual constant force mechanisms display slight negative stiffness themselves in Fig. 3(*a*). This is not observed in simulation and is likely caused by manufacturing errors increasing the negative stiffness generated by the long plate spring. By tuning the length of the long plate spring, the slope can be increased or decreased even further [15].

For the CM with linear motion, we have significantly reduced device complexity and doubled relative range of motion compared to the state of the art [17,18] while maintaining a stiffness reduction between 98% and 99.5%. The total number of individual plate springs is reduced from 38 to 12 and relative range of motion doubled from 3.3% to 6.6%. Although no device dimensions are mentioned in Refs. [17,18], they are estimated from the reported range of motion and visible clearance. The rotary mechanism is the first of his kind, so no comparison with literature is made.

One can reversibly change between both states of stiffness by switching the multistable mechanisms. However, after the compliant configuration has been entered, it cannot return to the stiff configuration by manipulating the main stage in a quasi-static fashion. Transitioning back requires the constant force and torque mechanisms to be pulled apart by an amount that exceeds the threshold force of the bistable elements. However, this threshold can never be exceeded because the range of motion of the main stage is limited by the frame. Increased clearance may overcome this.

A relatively large difference in stiffness reduction between the linear and rotary mechanisms is observed, i.e., 98.75% versus 90.5%. This is easily understood from Figs. 3(*a*) and 3(*c*). The more sudden and severe increase in stiffness at the tails of the graph in Fig. 3(*a*) make the unpreloaded configuration in the linear case stiffer and hence a more dramatic decrease possible. In addition, the constant force behavior seems more linear compared to the constant torque behavior, making it less likely that two CTM exactly counteract each other when preloaded against each other. Shape optimization may improve our proposed CTM.

In general, the proposed devices may enhance the efficiency of compliant mechanisms, by reducing inherent stiffness in a permanent fashion. More specifically, they may revolutionize low-frequency sensor technology such as accelerometers and gravimeters [4], but also mechanical energy harvesters [21]. In addition, they may be fundamentally required to make devices such as compliant transmission mechanisms practically usable [7,22]. Although the proposed devices are on centimeter scale, their monolithic nature allows micromanufacturing such as photolithography and two-photon stereo lithography [35]. In such micro devices, a low stiffness configuration could be permanently activated by switching the multistable mechanisms with, for example, a probe station or embedded actuators.

5 Conclusion

In this article, we have demonstrated fully compliant statically balanced mechanisms with rectilinear and rotational kinematics that do not require preloading assembly. They are capable of

reversibly reducing linear and angular stiffness by 98.5% and 90.5% over 10 mm and 0.35 rad, respectively. The mechanism with linear motion significantly reduces device complexity by using 12 plate springs instead of 38 while doubling the relative range of motion compared to the state of the art.

These dramatically different states of stiffness are obtained by preloading two constant force and torque mechanisms against each other with a monolithically integrated bistable switch. Toggling the bistable switch engages and disengages static balance, effectively turning off and on stiffness. A constant force mechanism based on existing literature is used, while a new constant torque mechanisms is created based on the same principle.

The prototyped devices are on centimeter scale and 3D printed out of PLA by FDM. However, their monolithic nature enables miniaturization and micromanufacturing by photolithography and two-photon stereo lithography. In such microsystems, the low stiffness configuration can be activated by actuating the main stage once with high force. They may find applications in low-frequency sensor technology, energy harvesting, microcompliant transmissions or provide robustness of sensitive sensors during launches to space.

Acknowledgment

This research is conducted at the instigation of and with close collaboration of TAG Heuer Institute, La Chaux de Fonds, 2300 Switzerland, and its Director, Mr G. A.(Guy) Sémon, and received funding from TAG Heuer Institute.

Conflict of Interest

There are no conflicts of interest.

Data Availability Statement

The datasets generated and supporting the findings of this article are obtainable from the corresponding author upon reasonable request. The data and information that support the findings of this article are freely available here.[2] The authors attest that all data for this study are included in the paper.

References

[1] Kota, S., Joo, J., Li, Z., Rodgers, S. M., and Sniegowski, J., 2001, "Design of Compliant Mechanisms: Applications to Mems," Analog Int. Circuits Signal Process., **29**(1–2), pp. 7–15.
[2] Huang, H.-W., and Yang, Y.-J., 2012, "A Mems Bistable Device With Push-on–Push-Off Capability," J. Microelectromech. Syst., **22**(1), pp. 7–9.
[3] Qiu, J., Lang, J. H., and Slocum, A. H., 2001, "A Centrally-Clamped Parallel-Beam Bistable Mems Mechanism," Technical Digest MEMS 2001 14th IEEE International Conference on Micro Electro Mechanical Systems (Cat. No. 01CH37090), Interlaken, Switzerland, Jan. 25, IEEE, pp. 353–356.
[4] Middlemiss, R., Samarelli, A., Paul, D., Hough, J., Rowan, S., and Hammond, G., 2016, "Measurement of the Earth Tides With a MEMS Gravimeter," Nature, **531**(7596), pp. 614–617.
[5] Luharuka, R., and Hesketh, P. J., 2007, "Design of Fully Compliant, In-Plane Rotary, Bistable Micromechanisms for Mems Applications," Sens. Actuators., A., **134**(1), pp. 231–238.
[6] Mayyas, M., and Stephanou, H., 2009, "Electrothermoelastic Modeling of Mems Gripper," Microsyst. Technol., **15**(4), pp. 637–646.
[7] Farhadi Machekposhti, D., Herder, J. L., and Tolou, N., 2019, "Frequency Doubling in Elastic Mechanisms Using Buckling of Microflexures," Appl. Phys. Lett., **115**(14), p. 143503.
[8] Stapel, A., and Herder, J. L., 2004, "Feasibility Study of a Fully Compliant Statically Balanced Laparoscopic Grasper," ASME 2004 International Design Engineering Technical Conferences and Computers and Information in Engineering Conference, Salt Lake City, Utah, USA, Sept. 28–Oct. 2, American Society of Mechanical Engineers, pp. 635–643.
[9] Tolou, N., and Herder, J. L., 2009, "Concept and Modeling of a Statically Balanced Compliant Laparoscopic Grasper," ASME 2009 International Design Engineering Technical Conferences and Computers and Information in Engineering Conference, San Diego, CA, Aug. 30–Sept. 2, American Society of Mechanical Engineers, pp. 163–170.
[10] de Lange, D. J., Langelaar, M., and Herder, J. L., 2008, "Towards the Design of a Statically Balanced Compliant Laparoscopic Grasper Using Topology Optimization," ASME 2008 International Design Engineering Technical Conferences and Computers and Information in Engineering Conference, Brooklyn, NY, Aug. 3–6, American Society of Mechanical Engineers, pp. 293–305.
[11] Lassooij, J., Tolou, N., Tortora, G., Caccavaro, S., Menciassi, A., and Herder, J., 2012, "A Statically Balanced and Bi-Stable Compliant End Effector Combined With a Laparoscopic 2DOF Robotic Arm," Mech. Sci., **3**(2), pp. 85–93.
[12] Tolou, N., Gallego, J., and Herder, J., 2010, "Statically Balanced Compliant Micro Mechanisms (sb-mems): A Breakthrough in Precision Engineering," Mikroniek, **50**(6), pp. 20–25.
[13] te Riele, F. L., and Herder, J. L., Sept. 2001, "Perfect Static Balance With Normal Springs," Proceedings of the 2001 ASME Design Engineering Technical Conferences, Pittsburg, PA, Sept. 9–12, pp. 9–12.
[14] Morsch, F. M., and Herder, J. L., 2010, "Design of a Generic Zero Stiffness Compliant Joint," ASME 2010 International Design Engineering Technical Conferences and Computers and Information in Engineering Conference, Montreal, Quebec, Canada, Aug. 15–18, American Society of Mechanical Engineers, pp. 427–435.
[15] Kuppens, P. R., Herder, J. L., and Tolou, N., 2019, "Permanent Stiffness Reduction by Thermal Oxidation of Silicon," J. Microelectromech. Syst., **28**(5), pp. 900–909.
[16] Pluimers, P. J., Tolou, N., Jensen, B. D., Howell, L. L., and Herder, J. L., 2012, "A Compliant On/Off Connection Mechanism for Preloading Statically Balanced Compliant Mechanisms," ASME 2012 International Design Engineering Technical Conferences and Computers and Information in Engineering Conference, Chicago, IL, Aug. 12–15, American Society of Mechanical Engineers, pp. 373–377.
[17] Pluimers, P., 2012, "Design for Specified Stiffness in Precision Engineering," Ph.D. thesis, Delft University of Technology (TU Delft), Delft, Netherlands.
[18] Tolou, N., 2012, "Statically Balanced Compliant Mechanisms for MEMS and Precision Engineering," Ph.D. thesis, Delft University of Technology, Delft, The Netherlands.
[19] Chen, G., and Zhang, S., 2011, "Fully-Compliant Statically-Balanced Mechanisms Without Prestressing Assembly: Concepts and Case Studies," Mech. Sci, **2**(2), pp. 169–174.
[20] Barel, M., Machekposhti, D. F., Herder, J., Tolou, N., and Sitti, M., 2018, "Permanent Preloading by Acceleration for Statically Balancing MEMS Devices," 2018 International Conference on Reconfigurable Mechanisms and Robots (ReMAR), Delft, The Netherlands, June 20–22, IEEE, pp. 1–11.
[21] Han, M., Yuan, Q., Sun, X., and Zhang, H., 2014, "Design and Fabrication of Integrated Magnetic MEMS Energy Harvester for Low Frequency Applications," J. Microelectromech. Syst., **23**(1), pp. 204–212.
[22] Machekposhti, D. F., Herder, J. L., Sémon, G., and Tolou, N., 2018, "A Compliant Micro Frequency Quadrupler Transmission Utilizing Singularity," J. Microelectromech. Syst., **27**(3), pp. 506–512.
[23] Hoetmer, K., Herder, J. L., and Kim, C. J., 2009, "A Building Block Approach for the Design of Statically Balanced Compliant Mechanisms," ASME 2009 International Design Engineering Technical Conferences and Computers and Information in Engineering Conference, San Diego, CA, Aug. 30– Sept. 2, American Society of Mechanical Engineers, pp. 313–323.
[24] Xu, Q., 2017, "Design of a Large-Stroke Bistable Mechanism for the Application in Constant-Force Micropositioning Stage," ASME J. Mech. Rob., **9**(1), p. 011006.
[25] Tolou, N., Pluimers, P., Jensen, B. D., Magleby, S., Howell, L., and Herder, J. L., 2011, "Constant Force Micro Mechanism Out of Carbon Nanotube Forest," Proceedings of the 12th EUSPEN International Conference, Stockholm, Sweden, June.
[26] Hou, C.-W., and Lan, C.-C., 2013, "Functional Joint Mechanisms With Constant-Torque Outputs," Mech. Mach. Theory., **62**, pp. 166–181.
[27] Nair Prakashah, H., and Zhou, H., 2016, "Synthesis of Constant Torque Compliant Mechanisms," ASME J. Mech. Rob., **8**(6), p. 064503.
[28] Hopkins, J. B., and Culpepper, M. L., 2010, "Synthesis of Multi-Degree of Freedom, Parallel Flexure System Concepts Via Freedom and Constraint Topology (Fact)—Part I: Principles," Precis. Eng., **34**(2), pp. 259–270.
[29] Hopkins, J. B., and Culpepper, M. L., 2010, "Synthesis of Multi-Degree of Freedom, Parallel Flexure System Concepts Via Freedom and Constraint Topology (Fact). Part II: Practice," Precis. Eng., **34**(2), pp. 271–278.
[30] Zirbel, S. A., Tolman, K. A., Trease, B. P., and Howell, L. L., 2016, "Bistable Mechanisms for Space Applications," PLoS One., **11**(12), p. e0168218.
[31] Qiu, J., Lang, J. H., and Slocum, A. H., 2004, "A Curved-Beam Bistable Mechanism," J. Microelectromech. Syst., **13**(2), pp. 137–146.
[32] Berntsen, L., Gosenshuis, D. H., and Herder, J. L., 2014, "Design of a Compliant Monolithic Internally Statically Balanced Four-Bar Mechanism," ASME 2014 International Design Engineering Technical Conferences and Computers and Information in Engineering Conference, Buffalo, NY, Aug. 17–20, American Society of Mechanical Engineers, p. V05AT08A040.
[33] Luharuka, R., and Hesketh, P. J., 2008, "A Bistable Electromagnetically Actuated Rotary Gate Microvalve," J. Micromech. Microeng., **18**(3), p. 035015.
[34] Casavola, C., Cazzato, A., Moramarco, V., and Pappalettere, C., 2016, "Orthotropic Mechanical Properties of Fused Deposition Modelling Parts Described by Classical Laminate Theory," Mater. Des., **90**, pp. 453–458.
[35] Chizari, S., Shaw, L. A., and Hopkins, J. B., 2019, "Simultaneous Printing and Deformation of Microsystems Via Two-Photon Lithography and Holographic Optical Tweezers," Mater. Horiz., **6**(2), pp. 350–355.

[2]https://youtu.be/NlZd98ubJbY, https://youtu.be/BVvEcgl4HR0, https://youtu.be/M5PKK63LkD0, https://youtu.be/vkpembB9J˙s.